Stability analysis of shallow wake flows

By A. A. KOLYSHKIN[1]† AND M. S. GHIDAOUI[2]‡

[1]Department of Engineering Mathematics, Riga Technical University, Riga, Latvia LV 1048
[2]Department of Civil Engineering, The Hong Kong University of Science & Technology,
Kowloon, Hong Kong

Experimentally observed periodic structures in shallow (i.e. bounded) wake flows are believed to appear as a result of hydrodynamic instability. Previously published studies used linear stability analysis under the rigid-lid assumption to investigate the onset of instability of wakes in shallow water flows. The objectives of this paper are: (i) to provide a preliminary assessment of the accuracy of the rigid-lid assumption; (ii) to investigate the influence of the shape of the base flow profile on the stability characteristics; (iii) to formulate the weakly nonlinear stability problem for shallow wake flows and show that the evolution of the instability is governed by the Ginzburg–Landau equation; and (iv) to establish the connection between weakly nonlinear analysis and the observed flow patterns in shallow wake flows which are reported in the literature. It is found that the relative error in determining the critical value of the shallow wake stability parameter induced by the rigid-lid assumption is below 10% for the practical range of Froude number. In addition, it is shown that the shape of the velocity profile has a large influence on the stability characteristics of shallow wakes. Starting from the rigid-lid shallow-water equations and using the method of multiple scales, an amplitude evolution equation for the most unstable mode is derived. The resulting equation has complex coefficients and is of Ginzburg–Landau type. An example calculation of the complex coefficients of the Ginzburg–Landau equation confirms the existence of a finite equilibrium amplitude, where the unstable mode evolves with time into a limit-cycle oscillation. This is consistent with flow patterns observed by Ingram & Chu (1987), Chen & Jirka (1995), Balachandar *et al.* (1999), and Balachandar & Tachie (2001). Reasonable agreement is found between the saturation amplitude obtained from the Ginzburg–Landau equation under some simplifying assumptions and the numerical data of Grubišić *et al.* (1995). Such consistency provides further evidence that experimentally observed structures in shallow wake flows may be described by the nonlinear Ginzburg–Landau equation. Previous works have found similar consistency between the Ginzburg–Landau model and experimental data for the case of deep (i.e. unbounded) wake flows. However, it must be emphasized that much more information is required to confirm the appropriateness of the Ginzburg–Landau equation in describing shallow wake flows.

1. Introduction

Shallow wake flows are flows behind obstacles (such as islands and headlands), where the transverse length scale of the flow, D, is much larger than the water

† Currently a visiting scholar at the Department of Civil Engineering, The Hong Kong University of Science & Technology, Kowloon, Hong Kong.
‡ Author to whom correspondence should be addressed.

depth, H (i.e. $D/H \gg 1$). Satellite images and aeronautical photographs show the formation of eddies in the lee of islands and headlands (Wolanski, Imberger & Heron 1984; Ingram & Chu 1987). Photograph number 173 in Van Dyke (1982) provides an excellent flow visualization of a shallow wake flow past an obstacle, where the visualization material is oil and the obstacle is the leaking tanker Argo Merchant which went aground on the Nantucket shoals in 1976 and settled at a 45° angle to the current. To an observant hydrodynamicist, this photo not only shows an environmental disaster, it also displays the striking difference between shallow wake flow and the well-studied unbounded wake flow: although the Reynolds number of the flow in the Nantucket disaster is 10^7 (Van Dyke 1982), the leaking oil displays a von Kármán vortex street (i.e. sinuous form) flow pattern. Recall that the von Kármán vortex street in unbounded flows is limited to Reynolds numbers much smaller than 10^7.

The flow pattern of water in the wake of islands exhibits a complex eddy-like motion. Field, laboratory and theoretical studies show that these eddies create complex flows which can trap sediments and pollutants and thus create poor water quality on the sheltered side of islands. Therefore, the understanding of island wake flow is important in terms of water quality and plays a decisive factor in the location of outfall discharges, mud disposal, cooling intakes, marine parks and reserves. In addition, trapping of contaminants and sediment can have detrimental economic effects on the marine culture industry in Hong Kong, for example. While islands and headlands provide shelter for the marine culture from the prevailing winds (i.e. high waves), poor water quality conditions induced by the eddies in the wakes of islands and headlands can result in fish disease and mortality. During the summer of 1994, it is believed that the trapping of low-salinity Pearl River water in sheltered areas caused intense stratification and resulted in extensive seabed killings in Hong Kong.

In view of their prominence in nature and their practical importance, shallow wake flows have been analysed in the literature both experimentally and theoretically. Different flow patterns have been observed in aerial photographs behind islands in the sea and around mountains in the atmosphere (Wolanski *et al.* 1984; Ingram & Chu 1987). Shallow two-dimensional turbulent wake flows are studied experimentally by Chen & Jirka (1995), Lloyd & Stansby (1997), Balachandar, Ramachandran & Tachie (2000), Balachandar & Tachie (2001) and Tachie & Balachandar (2001). Chen & Jirka (1995) showed experimentally that there are three different types of shallow wakes: vortex shedding, unsteady bubble and steady bubble. It was found that the flow patterns behind circular cylinders and flat plates depend mainly on a shallow wake stability parameter $S = c_f D/H$, introduced in earlier paper by Ingram & Chu (1987), where c_f is the bottom friction coefficient and D is the width or diameter of a bluff body.

Analysis of flows behind obstacles in shallow water by Chen & Jirka (1995) and Ingram & Chu (1987) indicates that the development of the wakes is different from the wakes in deep water. First, limited water depth prevents the development of three-dimensional instabilities typical of wakes in deep water for sufficiently large Reynolds numbers. Second, bottom friction acts as a mechanism for suppression of the transverse growth of disturbances. Experiments conducted by Chen & Jirka (1995) confirm that the stabilization of large-scale motion occurs either in the near wake or later within the far wake.

Theoretical investigations of the structure of shallow water flows behind bluff bodies and their stability have been carried out by several authors (Chu, Wu &

Khayat 1991; Schär & Smith 1993*a*, *b*; Grubišić, Smith & Schär 1995; Chen & Jirka 1997; Yakubenko & Shugai 1999; Ghidaoui & Kolyshkin 1999). It was found that the stability characteristics of shallow water flows depend on the magnitude of the bed-friction number which characterizes the ratio of the bed-friction dissipation term to the production term. Since the shallow wake patterns resemble two-dimensional wake patterns observed in flows behind a cylinder at low Reynolds number, the concepts of convective and absolute instability used to classify wake patterns at low Reynolds number (Huerre & Monkewitz 1990; Monkewitz 1988) were also applied by Chen & Jirka (1997) in an attempt to describe experimentally observed shallow wake flows at high Reynolds number. Chen & Jirka (1997) used two-dimensional depth-averaged shallow-water equations with the rigid-lid assumption to study convective and absolute instability of shallow wakes. They derived the modified Orr–Sommerfeld equation with additional terms that represent bottom friction (and the modified Rayleigh equation for the inviscid case). Chen & Jirka (1997) also made comparison between theoretical results and their experimental data (Chen & Jirka 1995). They found that stability characteristics of the flow are in qualitative agreement with experimental data.

The linear stability theory gives an indication of when a particular flow becomes unstable and can be used to describe the structure of the critical motion which takes place just above the threshold. However, the linear theory cannot predict the evolution of the disturbance above the threshold. In order to study the further development of instability one needs to use a nonlinear approach. Weakly nonlinear theories (Stewarston & Stuart 1971; Huerre & Rossi (1998)) are used to develop an evolution equation for the most unstable mode. One of the popular dynamical models which is used to study nonlinear flow dynamics is the Ginzburg–Landau equation. It is shown, for example, in Provansal, Mathis & Boyer (1987), Schumm, Berger & Monkewitz (1994) and Leweke & Provansal (1995) that the Ginzburg–Landau equation can be successfully used to describe experimental observations of flow behind bluff bodies for a wide range of Reynolds numbers. The coefficients of the Ginzburg–Landau equation are determined from experimental data. Hence, in this case, it is used as a model equation and the problem of deriving this equation from hydrodynamic equations is still an open problem for flows behind bluff bodies.

To the authors' knowledge, the first paper where the Ginzburg–Landau equation was derived from the Navier–Stokes equations for the case of a plane Poiseuille flow was Stewartson & Stuart (1971). Recently Feddersen (1998) used a weakly nonlinear approach to study the evolution of shear waves in near-shore flows. The method of multiple scales is used in their papers (see, for example, Kevorkian & Cole 1996) to derive the amplitude evolution equation for the most unstable mode.

Thus, the Ginzburg–Landau equation is used in the literature in two ways: first, as a phenomenological model and second, as an equation which appears naturally in many hydrodynamical applications when weakly nonlinear analysis is used. This paper shows that, for the case of shallow wake flows, the Ginzburg–Landau equation does not have to be assumed; it can be derived from the rigid-lid shallow-water equations.

The present paper is devoted to the analytical and numerical study of the linear and weakly nonlinear stability of flows in shallow wakes. Where possible, the connection between stability theory and observed features reported in the literature is sought. The paper is organized as follows. First, the accuracy of the rigid-lid assumption

for the case of wake flows is evaluated. The results of linear stability calculations show that the error in using the rigid-lid assumption for calculation of critical values of the stability parameter does not exceed 10%. Second, the influence of the shape of the velocity profile on the absolute and convective stability boundary is investigated. Third, weakly nonlinear analysis is used to derive an amplitude evolution equation above the threshold. It is shown that the evolution equation is the complex Ginzburg–Landau equation. The coefficients of the equation are calculated. It is found that for one set of the parameters the Landau constant is negative and therefore a finite-amplitude equilibrium is possible. This is consistent with the patterns observed by Ingram & Chu (1987), Chen & Jirka (1995), Balachandar, Tachie & Chu (1999), and Balachandar & Tachie (2001).

2. Linear stability analysis

2.1. *Influence of the Froude number on the stability characteristics*

In this section some estimates of the accuracy of the rigid–lid assumption are provided. Under the rigid-lid assumption the system of shallow water equations can be reduced to a single equation where the unknown function is the stream function of the flow. Weakly nonlinear theory applied to this equation results in a single-amplitude evolution equation of Gizburg–Landau type. Hence, the accuracy of the rigid-lid assumption needs to be analysed in order to justify the weakly nonlinear analysis. Since one of the major objectives of the paper is to derive and analyse an amplitude equation which describes the transition from a stable to convectively unstable wake, we are mainly interested in the convective instability boundary. The influence of the Froude number on the convective stability characteristics of the flow is investigated numerically. In addition, experimental data of Chen & Jirka (1995) are used in an attempt to justify the use of the rigid-lid assumption for the calculation of the absolute instability boundary.

The two-dimensional inviscid shallow-water equations are (e.g. Chaudhry 1993; Liggett 1994):

$$\frac{\partial H}{\partial T} + \frac{\partial}{\partial X}(UH) + \frac{\partial}{\partial Y}(VH) = 0, \tag{1}$$

$$\frac{\partial U}{\partial T} + U\frac{\partial U}{\partial X} + V\frac{\partial U}{\partial Y} + g\frac{\partial H}{\partial X} - gS_{0x} + c_f\frac{U\sqrt{U^2+V^2}}{2H} = 0, \tag{2}$$

$$\frac{\partial V}{\partial T} + U\frac{\partial V}{\partial X} + V\frac{\partial V}{\partial Y} + g\frac{\partial H}{\partial Y} - gS_{0y} + c_f\frac{V\sqrt{U^2+V^2}}{2H} = 0, \tag{3}$$

where X and Y are the spatial coordinates, T is the time, U and V are the depth-averaged velocity components in the X- and Y-directions, respectively, $S_{0x} = -\partial z_b(x, y)/\partial x$ and $S_{0y} = -\partial z_b(x, y)/\partial y$ are the bed slopes, $z_b(x, y)$ is the vertical distance from an arbitrary datum to the bed of the flow, H is the water depth, c_f is the friction coefficient such that the wall shear along the x- and y-directions is $\tau_{wx} = \frac{1}{2}c_f\rho U\sqrt{U^2+V^2}$ and $\tau_{wy} = \frac{1}{2}c_f\rho V\sqrt{U^2+V^2}$, respectively. Semi-empirical formulae for evaluation of c_f can be found in Schlichting (1979).

Let the scale for length, time and velocity be b, b/U_a and U_a, respectively, where b is some characteristic length scale (which will be defined later) and U_a is the ambient velocity. Then equations (1)–(3) can be written in the following

dimensionless form:

$$\frac{\partial h}{\partial t} + \frac{\partial}{\partial x}(uh) + \frac{\partial}{\partial y}(vh) = 0, \tag{4}$$

$$\frac{\partial u}{\partial t} + u\frac{\partial u}{\partial x} + v\frac{\partial u}{\partial y} + \frac{1}{Fr_b^2}\left(\frac{\partial h}{\partial x} - S_{0x}\right) + \frac{c_f u\sqrt{u^2 + v^2}}{2h} = 0, \tag{5}$$

$$\frac{\partial v}{\partial t} + u\frac{\partial v}{\partial x} + v\frac{\partial v}{\partial y} + \frac{1}{Fr_b^2}\left(\frac{\partial h}{\partial y} - S_{0y}\right) + \frac{c_f v\sqrt{u^2 + v^2}}{2h} = 0, \tag{6}$$

where x and y are the spatial coordinates, t is the time, u and v are the velocity components, h is the water depth and $Fr_b = U_a/\sqrt{gb}$ is a Froude-like number.

We assume that the base flow has the following structure:

$$\boldsymbol{u}_0 = (u_0(y), 0). \tag{7}$$

Consider a perturbed solution to equations (4)–(6) in the form

$$u = u_0(y) + u'(y)\,e^{-\lambda t + ikx}, \tag{8}$$

$$v = v'(y)\,e^{-\lambda t + ikx}, \tag{9}$$

$$h = \frac{H_0}{b} + h'(y)\,e^{-\lambda t + ikx}, \tag{10}$$

where H_0 is the undisturbed water depth, u', v' and h' are the complex amplitudes of the normal perturbations, k is the wavenumber and $\lambda = \lambda_r + i\lambda_i$ is a complex eigenvalue. Substituting (8)–(10) into equations (4)–(6) and linearizing the equations in the neighbourhood of the base flow we obtain the following system of ordinary differential equations for u', v' and h':

$$\frac{H_0}{b}\frac{dv'}{dy} + ikh'u_0 + ik\frac{H_0}{b}u' - \lambda h' = 0, \tag{11}$$

$$\frac{1}{Fr_b^2}\frac{dh'}{dy} + v'\left(u_0\frac{S}{2} + iku_0\right) - \lambda v' = 0, \tag{12}$$

$$u'(iku_0 + Su_0) + v'\frac{du_0}{dy} + h'\left(\frac{ik}{Fr_b^2} - u_0^2 S\frac{b}{2H_0}\right) - \lambda u' = 0 \tag{13}$$

with the boundary conditions

$$v'(\pm\infty) = 0, \tag{14}$$

where $S = c_f b/H_0$.

The system (11)–(13) together with the boundary conditions (14) forms an eigenvalue problem. The eigenvalues, $\lambda_s = \lambda_{rs} + i\lambda_{is}$, $s = 1, 2, \ldots$, determine the linear stability of the base flow described by (7). This base flow is said to be linearly stable if $\lambda_{rs} > 0$ for all s, and linearly unstable if $\lambda_{rs} < 0$ for at least one value of s. The numerical method for the solution of eigenvalue problem is described in detail in Ghidaoui & Kolyshkin (1999).

Some estimates of the influence of the Froude number on the stability boundary of transverse shear flows in shallow water flows are presented in Falqués & Iranzo (1994), Ghidaoui & Kolyshkin (1999) and Kolyshkin & Ghidaoui (2002). Falqués & Iranzo (1994) investigated the stability of a mean alongshore current in near-shore flows. They found that the error in the growth rates of disturbances due to the rigid-lid assumption for plane sloping beaches is 12% when the Froude number is

0.63 and 28% when the Froude number is 0.89. Ghidaoui & Kolyshkin (1999) and Kolyshkin & Ghidaoui (2002) studied the linear stability of transverse shear flows in compound and composite open channels. One of the widely used assumptions in the analysis of flows in open systems is the rigid-lid assumption. This assumption consists of replacing the gravity-driven free-surface flow by an equivalent pressure-driven flow between two parallel horizontal plates with the top plate being inviscid (acting like a lid) and the bottom plate having the same c_f as the original channel. The distance between the plates is equal to the original water height. By examining different base velocity profiles Ghidaoui & Kolyshkin (1999) showed that the rigid-lid assumption works well for weak shear flows and/or small Froude numbers. In addition, they showed that the rigid-lid equations are the limit of the shallow-water equations when the Froude number tends to zero. In the present paper we compare the results of linear stability calculations for the problem (11)–(14) with the results obtained with the rigid-lid assumption.

Two-dimensional dimensionless shallow-water equations under the rigid-lid assumption have the form

$$\frac{\partial u}{\partial x} + \frac{\partial v}{\partial y} = 0,$$ (15)

$$\frac{\partial u}{\partial t} + u\frac{\partial u}{\partial x} + v\frac{\partial u}{\partial y} + \frac{\partial p}{\partial x} + \frac{c_f}{2h}u\sqrt{u^2+v^2} = 0,$$ (16)

$$\frac{\partial v}{\partial t} + u\frac{\partial v}{\partial x} + v\frac{\partial v}{\partial y} + \frac{\partial p}{\partial y} + \frac{c_f}{2h}v\sqrt{u^2+v^2} = 0,$$ (17)

where p is the dimensionless pressure such that $\partial p/\partial x = -S_{0x}/Fr_b^2$ and $\partial p/\partial y = -S_{0y}/Fr_b^2$.

Using (8), (9) and a similar expression for the perturbation of pressure, and eliminating pressure p from (16), (17) we obtain the following modified Rayleigh equation for the function $v'(y)$:

$$(iku_0 + Su_0)\frac{d^2v'}{dy^2} + S\frac{du_0}{dy}\frac{dv'}{dy} - v'\left(ik\frac{d^2u_0}{dy^2} + ik^3u_0 + \tfrac{1}{2}Sk^2u_0\right) - \lambda\left(\frac{d^2v'}{dy^2} - k^2v'\right) = 0$$ (18)

with the boundary conditions (14).

The transverse velocity profile of a self-preserving unbounded wake for low Reynolds numbers can be approximated by the formula

$$u_0(y) = 1 + \frac{2R}{1-R}[1 + \sinh^{2N}(\alpha y)]^{-1},$$ (19)

where $R = (U_c - U_a)/(U_c + U_a)$ is the velocity ratio, $\alpha = \sinh^{-1}(1)$, U_c is the velocity on the centreline, $y = Y/b$, b is the wake half-width (which is defined as the distance from the axis of the wake such that $U(b) = \bar{U} = (U_c + U_a)/2$) and N is the 'shape' parameter, $N \geqslant 1$. The profile (19) is suggested by Monkewitz (1988) after careful analysis of available experimental data and it satisfactorily represents measured streamwise velocity distributions in the near wake of circular cylinders for small Reynolds numbers (up to $Re = 48.5$). Recent experimental results (Balanchandar & Tachie 2001) suggest that a similar velocity distribution can also be used for shallow water layers. The velocity distribution $u_0(y)$ given by (19) is shown in figure 1 for two values of N and three values of R. The curve for $N = 2$ is similar to the measured
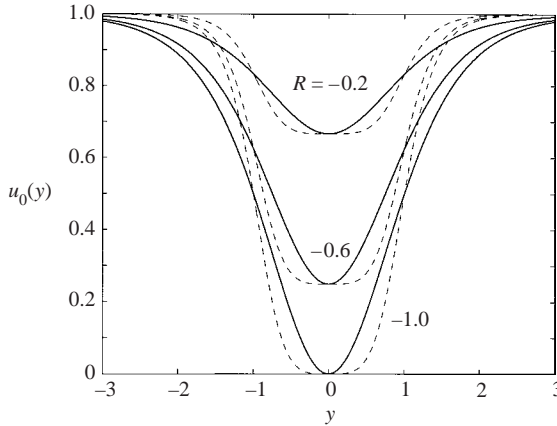
FIGURE 1. Base velocity profiles for different values of N. The solid and dashed lines correspond to the cases $N = 1$ and $N = 2$, respectively.
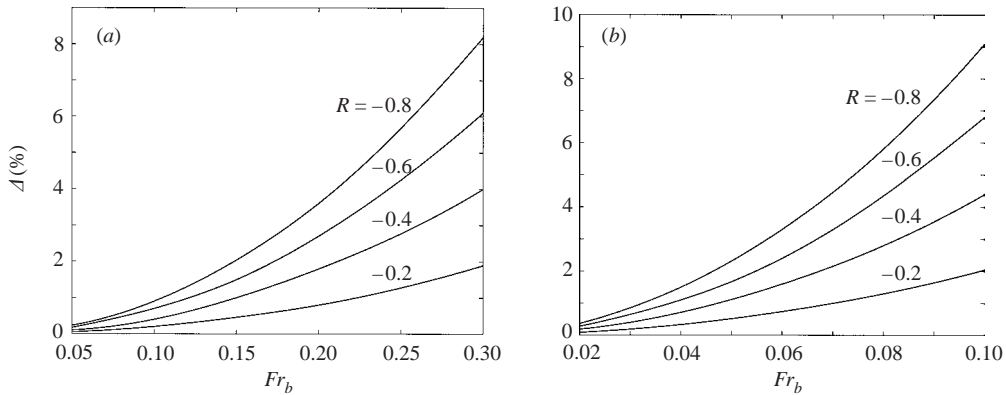

FIGURE 2. The percentage difference Δ between the values of S_c with and without the rigid-lid assumption for (a) the case $b/H_0 = 5$ and (b) $b/H_0 = 50$.

profile by Socolofsky, von Carmer & Jirka (2003) for the case of an unsteady bubble, while $N = 1$ is similar to the vortex street profile.

The rigid-lid assumption can be evaluated by solving problems (11)–(14) and (18), (14) numerically for different values of Froude number and other parameters of the problem that describe the base velocity profile (19) and comparing the critical values, S_c, of the parameter S. The set of all points in the (k, S)-plane for which one eigenvalue satisfies the condition $\lambda_r = 0$ while all other eigenvalues have positive real parts defines the neutral curve, $S_n(k)$. The critical value, S_c, of the stability parameter S is defined as the maximum, over all k, of the values $S_n(k)$ of S:

$$S_c = \max_k S_n(k). \tag{20}$$

Linear stability problems are solved by a pseudospectral collocation method based on Chebyshev polynomials (Ghidaoui & Kolyshkin 1999). The critical values of the stability parameter for finite Froude number Fr_b are compared with those for the rigid-lid assumption. The results of the comparison (in terms of the percentage difference) are shown in figures 2(a) and 2(b) for $N = 1$, $b/H_0 = 5$, $b/H_0 = 50$ and
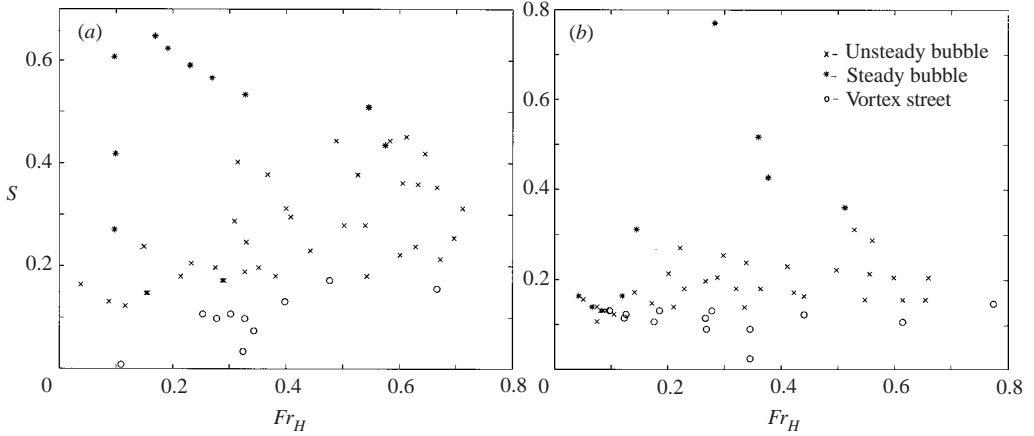
FIGURE 3. (*a*) Experimental classification of shallow wakes behind a circular cylinder and (*b*) a plate as a function of the Froude number. The data are computed from Chen & Jirka (1995), table 1 for (*a*) and table 2 for (*b*).

different values of R. These two values of b/H_0 are chosen since the condition $b/H_0 \gg 1$ is consistent with the shallow-water approximation. The Froude number Fr_H (based on the undisturbed water depth) is related to Fr_b by means of the formula $Fr_H = Fr_b \sqrt{b/H_0}$. In the experiments conducted by Chen & Jirka (1995) Fr_H was in the range 0.1–0.7 while in real island wakes Fr_H is about 0.1–0.2. In order to restrict consideration to values of Fr_H below 0.7, it is sufficient to choose Fr_b below 0.3 for the case $b/H_0 = 5$ and below 0.1 for the case $b/H_0 = 50$. Thus, the error in determining the critical value of the S parameter will be less than 10% as follows from figure 2. Taking into account experimental inaccuracy (Chen & Jirka reported that their experimental error is of the order 10%) it is safe to conclude that the rigid-lid assumption works well for calculation of the critical values of the parameter S for the range of Froude numbers typical for shallow wakes.

The concepts of absolute and convective instability are developed in the literature in order to describe spatio-temporal dynamics of perturbations and are used to classify different flow patterns in shallow wakes (Chen & Jirka 1997). Convective instability corresponds to the case when perturbations grow initially at any fixed location in the laboratory frame, but then eventually are swept away and disappear from the flow region. On the other hand, if perturbations grow exponentially in time at any fixed location in the laboratory frame, the instability is said to be absolute. In order to provide experimental evidence for the relative independence of the absolute instability boundary from the Froude number we have calculated the Froude number for all observations given in tables 1 and 2 in Chen & Jirka (1995). The results are shown in figures 3(*a*) and 3(*b*). The parameter S is defined $S = c_f D/H$, where D is the transverse body dimension, H is water depth and c_f is the bottom friction coefficient defined by semi-empirical formulae (see Schlichting 1979). For example, for smooth channels with $5000 \leqslant Re = U_a H/\nu \leqslant 3 \times 10^6$,

$$\frac{1}{\sqrt{c_f}} = -4 \log \left(\frac{1.25}{4 Re \sqrt{c_f}} \right).$$

For rough channels, c_f depends on both Re and the relative roughness coefficient. According to the classification presented in Chen & Jirka (1997) the transition
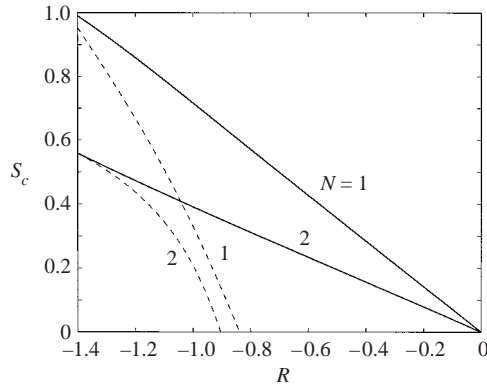
FIGURE 4. The critical values of the stability parameter S_c versus R for two values of N. The solid and dashed curves represent the convective and absolute instability boundary, respectively.

between a vortex street and an unsteady bubble corresponds to the transition from an absolutely unstable wake to a convectively unstable wake. Similarly, the transition from an unsteady bubble to a steady bubble corresponds to the transition from a convectively unstable to a stable wake.

As can be seen from the figure, the absolute instability boundary hardly depends on the Froude number; therefore one can expect to use the rigid-lid assumption for absolute instability calculations without any serious error. The computational proof of the relative independence of the convective instability boundary of the Froude number is given in figure 2. There is not enough experimental data to conclude that this boundary is not affected by the value of the Froude number. However, as mentioned above, theoretical results allow one to use the rigid-lid assumption within 10% error in the region $0 < Fr_H < 0.7$ and the rigid-lid assumption is adopted in the remainder of the paper.

2.2. *Influence of the shape of the velocity profile on the absolute and convective stability boundary*

Another set of computations is done in order to study the influence of the shape of the base velocity profile (19) on the stability characteristics of shallow wakes. Two basic approaches have been used in the literature in order to perform a linear stability analysis of unbounded wakes for low Reynolds numbers. The base velocity profile is chosen on the basis of experimental data (Monkewitz 1988; Triantafyllou, Triantafyllou & Chryssostomidis 1986) or is generated numerically using two-dimensional Navier–Stokes equations (Hannemann & Oertel 1989). In order to compare experimental data with the results of a linear stability analysis, Chen & Jirka (1997) used the maximum return velocity of the wake as the only link between experimental measurements and theoretical data. Although Chen & Jirka's theoretical results correctly predict the sequence of transitions in experimentally observed wake patterns, their experimental data do not match well with the predictions of the linear stability analysis.

In order to shed some light on this discrepancy a series of numerical experiments were performed with different values of R and N in (19). Note that in Chen & Jirka's (1997) paper the value of N was fixed at 1. The critical values of the stability parameter S_c are plotted against R in figure 4 for different values of N and R. The
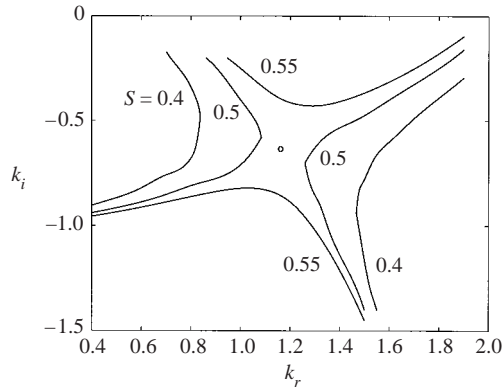
FIGURE 5. The curves $\lambda_r = 0$ for the shallow wake with the parameters $N = 2$, $R = -1.1$ and different values of S.

solid curves in figure 4 represent the dividing line between convectively unstable and stable wakes. It is seen from the figure that the critical values S_c are quite sensitive to the variation of the parameter N, that is, to the shape of the base velocity profile. These results clearly indicate that in order to compare experimental results with theoretical data from the linear stability analysis one needs to know not only the maximum return velocity of the wake but also the shape of the base velocity profile.

To distinguish between absolute and convective instabilities one has to perform an eigenvalue search for a saddle point in the (k, λ)-domain (see the relevant discussion in Huerre & Monkewitz 1990). In this case both the wavenumber and the eigenvalue are assumed to be complex of the form $k = k_r + ik_i$, $\lambda = \lambda_r + i\lambda_i$. In order to construct the dividing line between absolute and convective instabilities one assumes $\lambda_r = 0$ and performs an eigenvalue search for different k_r, k_i, R and S. A sample result of such calculations is shown in figure 5 where a family of curves corresponding to the case $\lambda_r = 0$ is constructed for different values of S (which are indicated on the figure). The values of N and R are fixed at 2 and -1.1, respectively. The saddle point (indicated as SP in figure 5) has the coordinates $k_r = 1.15$, $k_i = -0.63$ and corresponds to $S = 0.5075$. A similar search is performed for the values of R in the interval $(-1.4, 0)$ and the stability map is shown in figure 4. The dashed lines are the dividing lines between convective and absolute instabilities for two values of N, namely $N = 1$ and $N = 2$.

Chen & Jirka argued that the value $N = 1$ is chosen for their analysis because, as can be seen from the results for unbounded wakes (Monkewitz 1988), the critical Reynolds numbers change only slightly over the range $1 < N < 5$ if $R \leqslant -1$ and if $R \geqslant -1$ the wake flow approaches $N = 1$. It is seen from figure 4 that for unbounded wakes ($S = 0$) the values of R that divide regions of convective and absolute instabilities are close to each other ($R = -0.838$ for $N = 2$ and $R = -0.904$ for $N = 1$). However, as R decreases further, the difference between the critical values of the stability parameter S_c for two values of N is increasing. Thus one can conclude that the stability boundaries (both absolute and convective) are quite sensitive to the shape of the base velocity profile.

Finally, the location of the saddle points in the complex (k_r, k_i)-plane is shown in figure 6 for $N = 1$ and $N = 2$. It is seen from the figure that the spatial amplification rates at saddle points are quite different for the two velocity profiles with $N = 1$ and $N = 2$.
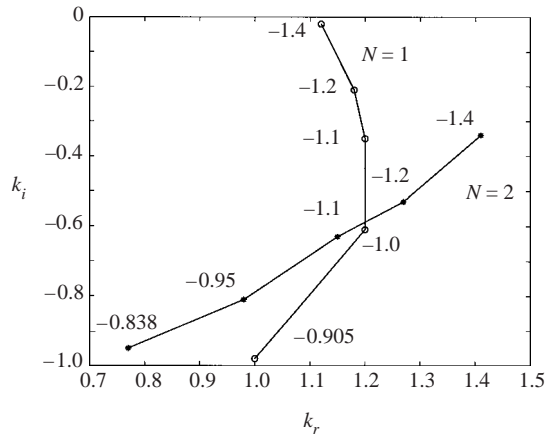
FIGURE 6. The loci of the saddle points in the (k_r, k_i)-plane for different values of R. The symbols $\circ$ and $*$ correspond to the cases $N = 1$ and $N = 2$, respectively.

3. Weakly nonlinear analysis

Linear analysis is used in the previous sections to define the onset of instability. The next natural step is to describe the nonlinear evolution of the most unstable linear mode in an attempt to reconcile the theoretical prediction with the observed shallow wake structures. It is believed that experimentally observed periodic structures in shallow wake flows (Ingram & Chu 1987; Chen & Jirka 1995; Balachandar *et al.* 1999) appear as a result of hydrodynamic instability. Balachandar *et al.* (1999) classify the flows as deep–shallow wakes and shallow–shallow wakes on the basis of the presence or absence of the vortex street. Experiments show that deep–shallow wake flow patterns closely resemble the structure of deep two-dimensional bluff-body wakes. The vortices in such cases are distinct and well organized; they increased in size downstream from the obstacle. The vortex street pattern is shown to be maintained over a large distance downstream (about 20 diameters for the experiments with a small cylinder in Chen & Jirka (1995) and about 200 plate widths for the experiments with a plate in Balachandar & Tachie (2001). Shallow–shallow wakes are characterized by relatively narrow wake regions. In addition, vortex street patterns either were not observed at all or appeared to be relatively weak and less organized in comparison with flows at larger depths. It is also found that the degree of variation from the classical vortex street flow increased downstream from the plate. Similar flow patterns were observed by Chen & Jirka (1995) (they classify the flows as vortex street, unsteady bubble and steady bubble).

Weakly nonlinear analysis has been found to be successful in describing the onset of periodicity in deep wake flows. The Landau equation is often used to model a supercritical Hopf bifurcation when a linearly unstable mode evolves with time into a limit-cycle oscillation. Mathis, Provansal & Boyer (1984) and Provansal *et al.* (1987) showed that the dynamics of deep water flow behind a cylinder can be described by the Landau equation. The coefficients of the Landau equation were calculated from experimental data for the range of Reynolds numbers near the threshold.

A global stability analysis performed by Noack & Eckelmann (1994) confirmed the experiments by Provansal *et al.* (1987), that is, the onset of periodicity is found to be described by the Landau equation. Reasonable agreement between the experimental and theoretical values of the coefficients of the Landau equation is found. Another

interesting conclusion from the experiments is that the growth rates and nonlinear frequency variations do not depend on the measuring point, in other words a single Landau equation can be used to describe the wake dynamics.

Taking into account some similarities between deep wake flows and shallow water flows weakly nonlinear theory is applied in this section to develop an evolution equation within the framework of the parallel flow assumption. Our analysis shows that the development of instability is governed by the complex Ginzburg–Landau equation (which reduces to the Landau equation if the amplitude A does not depend on the streamwise coordinate ξ).

Introducing the stream function $\psi(x, y, t)$ by the relations

$$u = \frac{\partial \psi}{\partial y}, \quad v = -\frac{\partial \psi}{\partial x}, \tag{21}$$

the system (15)–(17) of the shallow-water equations under the rigid-lid assumption can be rewritten in the form

$$(\Delta\psi)_t + \psi_y(\Delta\psi)_x - \psi_x(\Delta\psi)_y + \frac{c_f}{2h}\Delta\psi\sqrt{\psi_x^2 + \psi_y^2}$$
$$+ \frac{c_f}{2h\sqrt{\psi_x^2 + \psi_y^2}}\left(\psi_y^2\psi_{yy} + 2\psi_x\psi_y\psi_{xy} + \psi_x^2\psi_{xx}\right) = 0, \tag{22}$$

where Δ is the Laplace operator in two dimensions, the subscripts indicate the derivatives with respect to the variables x and y and the wake half-width b is chosen as the length scale. Note that the use of the rigid-lid assumption allows one to express the perturbed field in terms of a stream function and therefore obtain a single amplitude evolution equation as shown below. If the full system of shallow-water equations were used instead, the perturbed quantities could not be expressed in terms of the stream function alone and (independent) perturbations of u, v and h should be considered. As a result, a system of coupled nonlinear amplitude evolution equations of the Ginzburg–Landau type would emerge.

Consider a perturbed solution to (22) of the form

$$\psi = \psi_0 + \varepsilon\psi_1 + \varepsilon^2\psi_2 + \varepsilon^3\psi_3 + \dots \tag{23}$$

where ε is a small parameter and $\psi_{0y} = u_0$. Let us assume first that only two terms on the right-hand side of (23) are taken into account. Substituting (23) into (22) and collecting the terms of order ε we obtain

$$(\Delta\psi_1)_t + \psi_{0y}(\Delta\psi_1)_x - \psi_{1x}\psi_{0yyy} + S/2[\psi_{0y}\psi_{1xx} + 2\psi_{0y}\psi_{1yy} + 2\psi_{0yy}\psi_{1y}] = 0, \tag{24}$$

where $S = c_f b/H_0 = c_f/h$ is the stability parameter. Assuming that the perturbation $\psi(x, y, t)$ has the form

$$\psi_1(x, y, t) = \varphi_1(y)\exp[ik(x - ct)] + \text{c.c.} \tag{25}$$

(c.c. means 'complex conjugate') and substituting (25) into (24) we obtain

$$L_1\varphi_1 = 0, \tag{26}$$

where the operator L_1 is given by

$$L_1\varphi \equiv \varphi_{yy}\left(u_0 - c + \frac{Su_0}{ik}\right) + S\varphi_y\frac{u_{0y}}{ik} + \varphi\left(k^2c - k^2u_0 - u_{0yy} - \frac{u_0kS}{2i}\right). \tag{27}$$

One can see from (26) and (27) that equation (18) is recovered. The function φ_1 satisfies the boundary conditions

$$\varphi_1(\pm\infty) = 0. \tag{28}$$

The critical values of the parameters k, S and c for the case $N = 1$, $R = -0.5$ are $k_c = 0.926509$, $S_c = 0.195477$ and $c = 0.624193$, respectively, that is, the flow is stable if $S > 0.195477$ and convectively unstable if $S < 0.195477$. Here c denotes the wave speed at $k = k_c$ and $S = S_c$.

Weakly nonlinear theory (Stewartson & Stuart 1971) is used to analyse the effect of nonlinearities analytically. In accordance with the linear theory the most amplified mode at $S = S_c$, $k = k_c$ is given by (25) where the function $\varphi_1(y)$ is the eigenfunction of the linear stability problem and therefore can be replaced by $C\varphi_1(y)$, where the constant C cannot be determined from the linear stability theory. In order to study the nonlinear evolution of the most unstable mode (25) we restrict ourselves to the conditions around the point S_c, k_c. In particular, we assume that the parameter S is slightly below the critical value S_c, namely

$$S = S_c(1 - \varepsilon^2). \tag{29}$$

In this case the constant C is replaced by a slowly varying function of the spatial coordinate and time. The slow variation of this function in space and time can represent the wave packet. In particular, we introduce 'slow' time τ and stretched longitudinal coordinate ξ which moves with a group velocity c_g:

$$\tau = \varepsilon^2 t, \quad \xi = \varepsilon(x - c_g t).$$

Therefore, the stream function ψ is a function of x, t, ξ and $\tau : \psi = \psi(x, t, \xi(x, t), \tau(t))$. Using the chain rule, we obtain

$$\frac{\partial}{\partial t}\psi(x, t, \xi(x, t), \tau(t)) = \frac{\partial\psi}{\partial t} + \frac{\partial\psi}{\partial\xi}\frac{\partial\xi}{\partial t} + \frac{\partial\psi}{\partial\tau}\frac{\partial\tau}{\partial t}$$
$$= \frac{\partial\psi}{\partial t} - \varepsilon c_g\frac{\partial\psi}{\partial\xi} + \varepsilon^2\frac{\partial\psi}{\partial\tau}$$

and

$$\frac{\partial}{\partial x}\psi(x, t, \xi(x, t), \tau(t)) = \frac{\partial\psi}{\partial x} + \frac{\partial\psi}{\partial\xi}\frac{\partial\xi}{\partial x}$$
$$= \frac{\partial\psi}{\partial x} + \varepsilon\frac{\partial\psi}{\partial\xi}.$$

In this case the differential operators $\partial/\partial t$ and $\partial/\partial x$ are replaced by

$$\frac{\partial}{\partial t} \to \frac{\partial}{\partial t} - \varepsilon c_g\frac{\partial}{\partial\xi} + \varepsilon^2\frac{\partial}{\partial\tau} \tag{30}$$

and

$$\frac{\partial}{\partial x} \to \frac{\partial}{\partial x} + \varepsilon\frac{\partial}{\partial\xi}, \tag{31}$$

respectively. The function ψ_1 in (23) is sought in the form

$$\psi_1 = A(\xi, \tau)\varphi_1(y)\exp[ik_c(x - ct)] + \text{c.c.} \tag{32}$$

where c is the wave speed at $k = k_c$, $S = S_c$ and A is slowly varying amplitude.

In order to find the equation which describes the evolution of A one needs to consider higher terms of the perturbation expansion (23). Substituting (23) and (30)–(31) into (22) and collecting the terms of order ε gives

$$L\psi_1 = 0, \tag{33}$$

where the operator L is defined as

$$L\varphi \equiv \varphi_{xxt} + \varphi_{yyt} + \psi_{0y}\varphi_{xxx} + \psi_{0y}\varphi_{yyx} - \psi_{0yyy}\varphi_x + \tfrac{1}{2}S_c(\psi_{0y}\varphi_{xx} + 2\psi_{0yy}\varphi_y + 2\psi_{0y}\varphi_{yy}). \tag{34}$$

Collecting the terms of order ε^2 gives

$$\begin{aligned}
L\psi_2 = {} & c_g(\psi_{1xx\xi} + \psi_{1yy\xi}) - 2\psi_{1x\xi t} - 3\psi_{0y}\psi_{1xx\xi} - \psi_{1y}\psi_{1xxx} \\
& - \psi_{1y}\psi_{1yyx} - \psi_{0y}\psi_{1\xi yy} + \psi_{1x}\psi_{1xxy} + \psi_{1x}\psi_{1yyy} + \psi_{1\xi}\psi_{0yyy} \\
& - \tfrac{1}{2}S_c[\psi_{1xx}\psi_{1y} + 2\psi_{1x\xi}\psi_{0y} + 2\psi_{1yy}\psi_{1y} + 2\psi_{1x}\psi_{1xy} - 2\psi_{0y}\psi_{0yy}]. \tag{35}
\end{aligned}$$

Finally, collecting the terms of order ε^3 we obtain

$$\begin{aligned}
L\psi_3 = {} & c_g(\psi_{2xx\xi} + \psi_{2yy\xi} + 2\psi_{1x\xi\xi}) - \psi_{1xx\tau} - 2\psi_{2x\xi t} - \psi_{1\xi\xi t} - \psi_{1yy\tau} \\
& - 3u_0\psi_{2xx\xi} - 3u_0\psi_{1x\xi\xi} - \psi_{1y}\psi_{2xxx} - 3\psi_{1y}\psi_{1xx\xi} - \psi_{2y}\psi_{1xxx} - \psi_{2y}\psi_{1yyx} \\
& - \psi_{1y}\psi_{2yyx} - \psi_{1y}\psi_{1\xi yy} - u_0\psi_{2\xi yy} + \psi_{2x}\psi_{1xxy} + \psi_{1\xi}\psi_{1xxy} + \psi_{1x}\psi_{2xxy} \\
& + 2\psi_{1x}\psi_{1xy\xi} + \psi_{1x}\psi_{2yyy} + \psi_{2x}\psi_{1yyy} + \psi_{1\xi}\psi_{1yyy} + \psi_{2\xi}u_{0yy} \\
& - \tfrac{1}{2}S_c\left[\psi_{1xx}\psi_{2y} + \frac{3\psi_{1xx}\psi_{1x}^2}{2u_0} + \psi_{2xx}\psi_{1y} + 2\psi_{1\xi}\psi_{1y} + 2u_0\psi_{2x\xi} + u_0\psi_{1\xi\xi} \right. \\
& \left. + 2\psi_{1yy}\psi_{2y} + 2\psi_{2yy}\psi_{1y} - u_0\psi_{1xx} - 2u_{0y}\psi_{1y} - 2u_0\psi_{1yy} + 2\psi_{1x}\psi_{2xy} \right. \\
& \left. + 2\psi_{1x}\psi_{1\xi y} + 2\psi_{2x}\psi_{1xy} + 2\psi_{1\xi}\psi_{1xy} \right]. \tag{36}
\end{aligned}$$

The form of the right-hand side of (35) and the form of the function ψ_1 (see (32)) suggests that the function ψ_2 should be sought in the following form:

$$\psi_2 = AA^*\varphi_2^{(0)}(y) + A_\xi\varphi_2^{(1)}(y)\exp[ik_c(x - ct)] + A^2\varphi_2^{(2)}(y)\exp[2ik_c(x - ct)] + \text{c.c.} \tag{37}$$

where A^* denotes the complex conjugate of A, the subscripts denote the order of the approximation and the superscripts denote the index of the harmonic component. To explain, let us consider the linear terms with respect to ψ_1 on the right-hand side of (35):

$$c_g(\psi_{1xx\xi} + \psi_{1yy\xi}) - 2\psi_{1x\xi t} - 3\psi_{0y}\psi_{1xx\xi} - \psi_{0y}\psi_{1\xi yy} + \psi_{1\xi}\psi_{0yyy} - S_c\psi_{0y}\psi_{1x\xi}.$$

All the terms in the above expression contain the derivative with respect to ξ and are proportional to $\exp[ik_c(x - ct)]$ in accordance with (32). The operator L on the left-hand side of (35) does not contain derivatives with respect to ξ. Thus, we choose the solution $\psi_2^{(1)}$ which will balance the linear terms with respect to ψ_1 on the right-hand side of (35) in the form

$$\psi_2^{(1)} = A_\xi\varphi_2^{(1)}(y)\exp[ik_c(x - ct)].$$

Similarly one can explain the appearance of the other terms in (37).

Substituting (32) for ψ_1 and (37) for ψ_2 into (35) and collecting terms proportional to AA^* gives

$$\begin{aligned}
2S_c\left(u_0\varphi_{2yy}^{(0)} + u_{0y}\varphi_{2y}^{(0)}\right) = {} & ik_c(\varphi_{1y}\varphi_{1yy}^* - \varphi_{1y}^*\varphi_{1yy} + \varphi_1\varphi_{1yyy}^* - \varphi_1^*\varphi_{1yyy}) \\
& - \tfrac{1}{2}S_c[k_c^2(\varphi_1\varphi_{1y}^* + \varphi_1^*\varphi_{1y}) + 2(\varphi_{1y}^*\varphi_{1yy} + \varphi_{1yy}^*\varphi_{1y})] \tag{38}
\end{aligned}$$

with the boundary conditions

$$\varphi_2^{(0)}(\pm\infty) = 0. \tag{39}$$

Similarly, collecting the terms that are proportional to $A_\xi \exp[ik_c(x - ct)]$ yields

$$\varphi_{2yy}^{(1)}\left(u_0 - c + \frac{u_0 S_c}{ik_c}\right) + \frac{S_c u_{0y}}{ik_c}\varphi_{2y}^{(1)} + \varphi_2^{(1)}\left(k_c^2 c - k_c^2 u_0 - u_{0yy} - \frac{u_0 k_c S_c}{2i}\right)$$
$$= \frac{1}{ik_c}\varphi_1\left(-2k_c^2 c + 3k_c^2 u_0 + u_{0yy} - k_c^2 c_g - ik_c u_0 S_c\right) + \frac{1}{ik_c}(c_g - u_0)\varphi_{1yy} \tag{40}$$

with the boundary conditions

$$\varphi_2^{(1)}(\pm\infty) = 0. \tag{41}$$

It can be seen that the left-hand side of equation (40) is exactly the same as the left-hand side of equation (26) (if φ_1 is replaced by $\varphi_2^{(1)}$). Therefore, in accordance with Fredholm's alternative (see, for example, Zwillinger 1998), equation (40) has a solution if and only if its right-hand side is orthogonal to all eigenfunctions of the corresponding homogeneous adjoint problem.

The adjoint operator, L_1^a, and adjoint function φ_1^a of L_1^a are defined as follows:

$$\int_{-\infty}^{\infty} \varphi_1^a L_1(\varphi_1)\,dy = \int_{-\infty}^{\infty} \varphi_1 L_1^a(\varphi_1^a)\,dy. \tag{42}$$

Note that if φ_1 is an eigenfunction of the problem (26), (28), then both terms in (42) are equal to zero. This will also mean that φ_1^a is an eigenfunction of the adjoint problem and that the adjoint operator L_1^a must have the same spectrum as the operator L_1.

Integrating equation (26) by parts and using boundary conditions (28) we obtain the adjoint problem in the form

$$L_1^a \varphi_1^a = 0, \tag{43}$$

with the boundary conditions

$$\varphi_1^a(\pm\infty) = 0, \tag{44}$$

where

$$L_1^a \varphi_1^a \equiv \varphi_{1yy}^a(ik_c u_0 + S_c u_0) + \varphi_{1y}^a(2ik_c u_{0y} + S_c u_{0y})$$
$$+ \varphi_1^a\left(-ik_c^3 u_0 - \frac{u_0 k_c S_c}{2}\right) - ik_c c\left(\varphi_{1yy}^a - k_c^2 \varphi_1^a\right). \tag{45}$$

Hence, the solvability condition for equation (40) can be written in the form

$$\int_{-\infty}^{\infty} \varphi_1^a\left[\varphi_1\left(-2k_c^2 c + 3k_c^2 u_0 + u_{0yy} - k_c^2 c_g - ik_c u_0 S_c\right) + (c_g - u_0)\varphi_{1yy}\right]dy = 0. \tag{46}$$

Finally, collecting the terms proportional to $A^2 \exp[2ik_c(x - ct)]$ yields

$$[S_c u_0 + 2ik_c(u_0 - c)]\varphi_{2yy}^{(2)} + S_c u_{0y}\varphi_{2y}^{(2)} - \varphi_2^{(2)}\left[8ik_c^3(u_0 - c) + 2ik_c u_{0yy} + 2S_c k_c^2 u_0\right]$$
$$= ik_c(\varphi_1\varphi_{1yyy} - \varphi_{1y}\varphi_{1yy}) - \tfrac{1}{2}S_c\left(2\varphi_{1y}\varphi_{1yy} - 3k_c^2\varphi_1\varphi_{1y}\right) \tag{47}$$

with the boundary conditions

$$\varphi_2^{(2)}(\pm\infty) = 0. \tag{48}$$

The evolution of the amplitude A is determined from the terms of order ε^3. Equation (36) has a solution if and only if the right-hand side of (36) is orthogonal to

eigenfunction φ_1^a of the adjoint problem (43), (44). Multiplying the right-hand side of (36) by φ_1^a and integrating with respect to y from $-\infty$ to $+\infty$ we obtain the Ginzburg–Landau equation in the form

$$A_\tau = \sigma A + \delta A_{\xi\xi} + \mu |A|^2 A, \tag{49}$$

where the complex coefficients σ, δ and μ have the form

$$\sigma = \frac{\sigma_1}{\beta}, \quad \delta = \frac{\delta_1}{\beta}, \quad \mu = \frac{\mu_1}{\beta} \tag{50}$$

with

$$\beta = \int_{-\infty}^{\infty} \varphi_1^a \left(\varphi_{1yy} - k_c^2 \varphi_1 \right) \mathrm{d}y,$$

$$\sigma_1 = \tfrac{1}{2} S_c \int_{-\infty}^{\infty} \varphi_1^a \left(2u_0 \varphi_{1yy} + 2u_{0y} \varphi_{1y} - k_c^2 u_0 \varphi_1 \right) \mathrm{d}y,$$

$$\delta_1 = \int_{-\infty}^{\infty} \varphi_1^a \left[\varphi_{2yy}^{(1)}(c_g - u_0) + \varphi_2^{(1)} \left(-k_c^2 c_g - 2k_c^2 c + 3k_c^2 u_0 \right. \right.$$
$$\left. + u_{0yy} - ik_c u_0 S_c \right) + \varphi_1 \left(2ik_c c_g + ik_c c - 3ik_c u_0 - \tfrac{1}{2} u_0 S_c \right) \Big] \mathrm{d}y,$$

$$\mu_1 = \int_{-\infty}^{\infty} \varphi_1^a \Big\{ 6ik_c^3 \varphi_2^{(2)} \varphi_{1y}^* - 2ik_c \varphi_{1y}^* \varphi_{2yy}^{(2)} + 3ik_c^3 \varphi_1^* \varphi_{2y}^{(2)}$$
$$+ 2ik_c^3 \varphi_1 \varphi_{2y}^{(0)} - 2ik_c \varphi_{1yy} \varphi_{2y}^{(0)} + ik_c \varphi_{2y}^{(2)} \varphi_{1yy}^*$$
$$- ik_c \varphi_1^* \varphi_{2yyy}^{(2)} + 2ik_c \varphi_1 \varphi_{2yyy}^{(0)} + 2ik_c \varphi_{1yyy}^* \varphi_2^{(2)}$$
$$- \tfrac{1}{2} S_c \left[-2k_c^2 \varphi_1 \varphi_{2y}^{(0)} + 3k_c^2 \varphi_1^* \varphi_{2y}^{(2)} - \frac{3k_c^4}{2u_0} \varphi_1^2 \varphi_1^* \right.$$
$$\left. + 4\varphi_{1yy} \varphi_{2y}^{(0)} + 2\varphi_{1yy}^* \varphi_{2y}^{(2)} + 4\varphi_{1y} \varphi_{2yy}^{(0)} + 2\varphi_{2yy}^{(2)} \varphi_{1y}^* \right] \Big\} \mathrm{d}y. \tag{51}$$

Hence, in order to find the coefficients of the Ginzburg–Landau equation (49), one needs to find the critical values k_c, S_c and c from the solution of the linear stability problem (26), (28), find the corresponding eigenfunction φ_1, solve the adjoint problem (43), (44) and find the corresponding adjoint eigenfunction φ_1^a, solve three linear boundary-value problems (38)–(41), (47)–(48) and then evaluate the integrals (51).

4. Numerical results and discussion

A dispersion relation is defined at $S = S_c$ as the variation with k of the eigenvalue c of the differential equation (26) with boundary conditions (28):

$$\omega_c(k) + i\sigma_c(k) = kc, \tag{52}$$

where c is the critical eigenvalue. At $k = k_c$ the following conditions are satisfied:

$$\sigma_c(k_c) = 0, \quad \frac{\partial \omega_c(k_c)}{\partial k} = c_g, \quad \frac{\partial \sigma_c(k_c)}{\partial k} = 0, \tag{53}$$

where c_g is the group velocity. It is known (see, for example, Huerre & Rossi 1998) that in the neighbourhood of $k = k_c$ the dispersion relation (52) can be approximated by a parabola

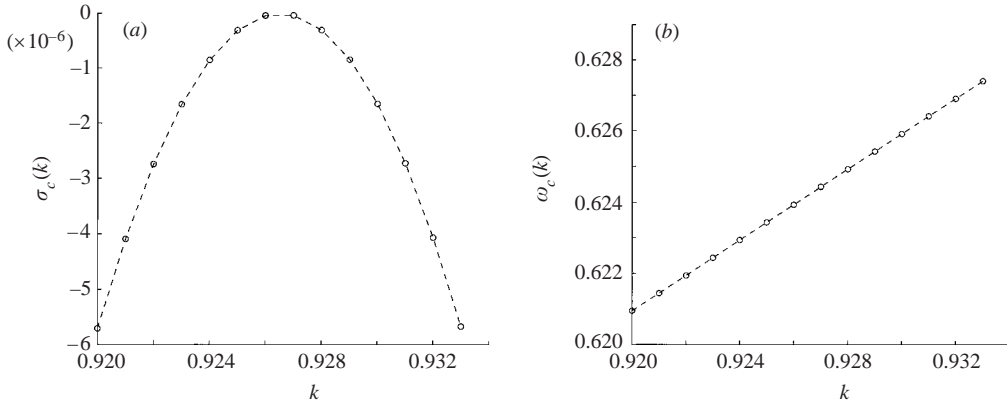$$\omega_c(k) + i\sigma_c(k) = a_0(k - k_c)^2 + a_1(k - k_c) + a_2. \tag{54}$$

FIGURE 7. The values of (*a*) σ_c and (*b*) ω_c near the critical wavenumber k_c. The circles represent calculated values. The dashed line is the best-fit parabola.
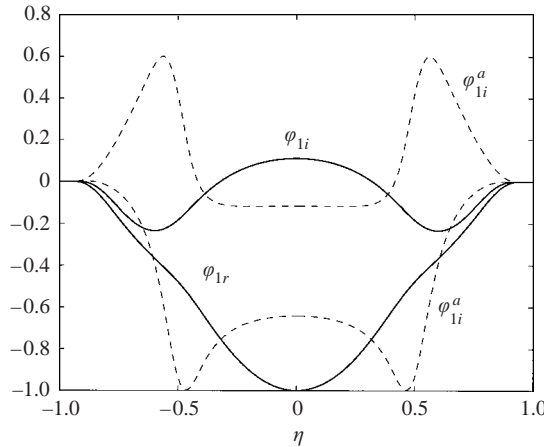

FIGURE 8. The real and imaginary parts of the function $\varphi_1(\eta)$ (solid lines) and the adjoint function $\varphi_1^a(\eta)$ (dashed lines) versus η.

The dispersion curve near the critical wavenumber $k_c = 0.926509$ is shown in figures 7(*a*) and 7(*b*). The circles represent calculated values while the solid lines are parabolas (54) obtained by the method of least-squares from the calculated values. In particular, we have

$$\omega_c(k) = -0.107631(k - 0.926509)^2 + 0.497022(k - 0.926509) + 0.624193, \qquad (55)$$

$$\sigma_c(k) = -0.13454(k - 0.926509)^2 + 1.3 \times 10^{-6}(k - 0.926509) + 2.5 \times 10^{-12}. \quad (56)$$

Since Chebyshev polynomials were used for calculations, the interval $-\infty < y < +\infty$ was mapped onto the interval $-1 < \eta < 1$ by means of the transformation $\eta = 2/\pi \arctan y$. The real and imaginary parts of the normalized eigenfunction $\varphi_1(\eta)$ and the adjoint eigenfunction $\varphi_1^a(\eta)$ are shown in figure 8. The graph of the main flow correction $\varphi_2^{(0)}(\eta)$ is presented in figure 9. Finally, the graphs of the real and imaginary parts of the functions $\varphi_2^{(1)}(\eta)$ and $\varphi_2^{(2)}(\eta)$ are given in figure 10.

It follows from (55)–(56) that all the conditions (53) are satisfied and that $c_g = 0.497022$. The group velocity calculated from the solvability condition (46) is
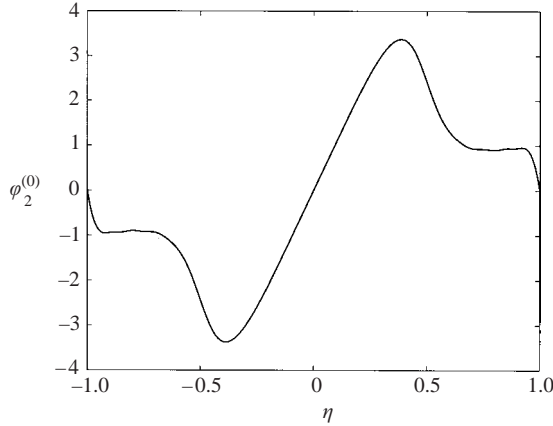
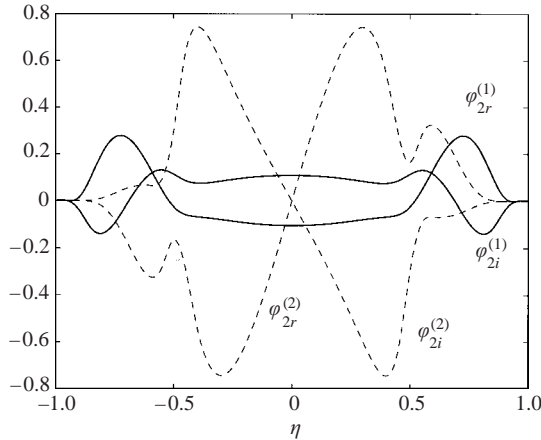FIGURE 9. The graph of the function $\varphi_2^{(0)}(\eta)$.

FIGURE 10. The real and imaginary parts of the function $\varphi_2^{(1)}(\eta)$ (solid lines) and $\varphi_2^{(2)}(\eta)$ (dashed lines) versus η.

equal to $c_g = 0.4970226 - i0.00000041$. As one can see, the two values of c_g agree well. Such a comparison is a useful check of algebra and numerical calculations. The coefficient δ in the Ginzburg–Landau equation can be calculated as follows (see Stewartson & Stuart 1971):

$$\delta = -\frac{1}{2}\frac{\partial^2 \sigma_c}{\partial k^2} + i\frac{1}{2}\frac{\partial^2 \omega_c}{\partial k^2}. \tag{57}$$

Using (55)–(57) we obtain

$$\delta = 0.13454 - i0.107631. \tag{58}$$

As another check of our results we calculated the coefficient δ using formula (51). The result is $\delta = 0.1345396 - i0.107573$. Again, the two values of δ are close to each other for both the real and imaginary parts.

The coefficients σ and μ in the Ginzburg–Landau equation are calculated from (51) and have the form

$$\sigma = 0.08989 + \text{i}0.00035, \quad \mu = -4.33700 - \text{i}9.49653. \tag{59}$$

Since the real part of μ is negative, finite-amplitude equilibrium is possible. This means that the Ginzburg–Landau equation (49) can describe a Hopf bifurcation (that is, the transition from a steady state to a limit cycle) at least within the framework of the parallel flow assumption. These results are in qualitative agreement with experimental observations by Chen & Jirka (1995) and Balachandar *et al.* (1999) where periodic structures are found for certain experimental conditions.

Grubišić *et al.* (1995) presented results of numerical simulations of shallow wake flows behind an obstacle (both linear stability results under some simplifying assumptions and nonlinear wake development are discussed). The calculations are performed in terms of the non-dimensional drag number r (which is related to S by the formula $S = 2r$) for different positions downstream of the obstacle. In particular, figure 9 in Grubišić *et al.* (1995) shows that for $S = 0.2$ a small finite velocity defect is present very far downstream (in the region $x_0 > 7$ where x_0 is the distance downstream from the centre of the obstacle). In addition, figure 10(*b*) in their paper (the graph of convective growth rate) shows that for $S = 0.2$ the flow is stable for $x_0 > 7.5$. Both results indicate the existence of a finite-amplitude equilibrium far downstream. The value of the parameter $U_c/U_a - 1$ at $x_0 = 7$ (as follows from figure 9(*c*) of Grubišić *et al.* 1995) is about -0.6 and it is gradually increasing to zero as x_0 increases. On the other hand, $U_c/U_a - 1 = -0.6$ corresponds to $R = -0.43$. This value of R is close to the one used in our weakly nonlinear calculations, namely $R = -0.5$, and the corresponding value of S_c is $S_c = 0.195477$. A qualitative comparison of the base velocity profiles reported in Grubišić *et al.* (1995) with those plotted in figure 1 shows that the set of profiles in Grubišić *et al.* (1995) can be approximated by (19) with the value of N close to 1. However, no attempt was made at this stage to find the exact value of N corresponding to the profiles reported in Grubišić *et al.* (1995).

Grubišić *et al.* (1995) also determined the amplitude of the cross-stream velocity component at saturation as a function of both the non-dimensional drag number r and the position downstream of the obstacle. The maximum saturation amplitudes for $S = 0, 0.04, 0.08, 0.12, 0.16, 0.2$ are about 1.0, 0.8, 0.5, 0.2, 0.05, and 0, respectively. Therefore, the critical bed friction number for the numerical experiments of Grubišić *et al.* (1995) is $S_c = 0.2$. Since $S_c = 0.2$ and $S_c = 0.195477$ are very close in magnitude, comparisons between the data of Grubišić *et al.* (1995) and the weakly nonlinear analysis can be performed.

In order to compare the results of nonlinear model in Grubišić *et al.* (1995) with the Ginzburg–Landau model we make the following simplifying assumption. Consider an equilibrium state $A_\tau = 0$ and $A_{\xi\xi} = 0$ which results from the along-stream evolution of the flow in the limit $\xi \to \infty$ and $\tau \to \infty$. It then follows from (49) that an equilibrium amplitude $|A|_e = \sqrt{-\sigma_0/\mu_0}$ will be reached. In particular, the amplitude of cross-flow velocity at saturation is $A_s = k_c|A|_e = 0.9265\sqrt{0.08989/4.337} = 0.13$. That is, the model predicts that decreasing the value of S by a small amount below 0.195477 leads to a limit cycle with an amplitude of 0.13. The data of Grubišić *et al.* (1995) show that $A_s = 0.14$ when $S = 0.14$. This result shows some degree of consistency of the weakly nonlinear results with the numerical data of Grubišić *et al.* (1995) since the saturation amplitude is, indeed, achieved when the value of $S = 0.14$ is smaller than but close to the critical value of $S_c = 0.195477$. While encouraging, this preliminary agreement

between the numerical data of Grubišić *et al.* (1995) and the Ginzburg–Landau model does not constitute a proof that the Ginzburg–Landau equation correctly describe shallow water flows. A full spatio-temporal analysis of wake flows is necessary for complete verification of the Ginzburg–Landau model. Recent results (see, for example, Pier 2002) indicate that a combination of nonlinear analysis and methods of stability theory can be a powerful tool for investigation of spatio-temporal dynamics of wake flows.

More detailed experiments similar to those reported by Provansal *et al.* (1987) and Leweke & Provansal (1995) are needed for the case of shallow wakes in order to validate the Ginzburg–Landau model experimentally. In particular, transient shallow wake experiments where the flow is accelerated from a stable state to an unstable state are needed. Such experiments provide detailed spatial and temporal data of the along-stream and across-stream velocity perturbations associated with the development of the instability from its inception to its saturation. This information is essential for determining the parameters of the Ginzburg–Landau equation and for assessing the validity of this nonlinear equation in modelling flow instabilities and bifurcation in shallow shear flows.

It is clear that the identification of the parameters in (49) and the validation of this equation requires laboratory measurements of $|A|$ versus t. The amplitude $|A|$ is related to the amplitude of oscillations in the cross-stream and along-stream velocities by means of (21) and (32).

To obtain $|A|$ versus t measurements the flow must be accelerated from an initial bed friction number S_i, to a final bed friction number S_f, such that $S_f < S_c < S_i$. That is, S_f needs to be small enough so that the saturation regime (limit cycle) is well established. To ensure enough time for the instability to develop and reach the limit cycle it is important that the time scale of the acceleration is significantly larger than $1/\sigma_0$. The data should be collected at a few points downstream of the obstacle and should be repeated for different obstacle geometry. It must be noted here that the experimental verification of the Ginzburg–Landau requires much more data than the Landau equation due to the presence of diffusion in (49).

5. Conclusion

The flow pattern of water in the wake of islands exhibits a complex eddy-like motion. Field, laboratory and theoretical studies show that these eddies create complex flows which can trap sediments and pollutants and thus create poor water quality on the sheltered side of islands. As mentioned in the Introduction, the understanding of island wake flow is important in terms of water quality.

Stability theory can help in understanding the onset and the development of the experimentally observed periodic structures in shallow wake flows (Ingram & Chu 1987; Chen & Jirka 1995; Balachandar *et al.* 1999). Previously published studies used linear stability analysis under the rigid-lid assumption to investigate the onset of instability of wakes in shallow water flows. The present work evaluates the accuracy of the rigid-lid assumption. It is found that the error in calculating the critical value of the shallow wake stability parameter S introduced by the rigid-lid assumption is below 10% for the practical range of Froude number (i.e. $Fr_H \leqslant 0.7$). Therefore, the rigid-lid shallow-water equations form an appropriate model for shallow wakes and the flow structure is defined by the bed-friction number with the Froude number playing a minor role. It must be pointed that the influence of the Froude number on the stability results becomes apparent once it exceeds 1.0. Therefore, it is important

that investigators ensure that the Froude number is kept within the practical range (i.e. small).

The shape of obstacles (e.g. islands and headlands) is reflected in the shape of the wake velocity profile. To gain an appreciation of the sensitivity of the stability characteristics to the shape of the obstacle, the linear stability problem for different base flow profiles is investigated. It is shown that the shape of the velocity profile has a large influence on the stability characteristics of shallow wakes. Therefore, future experimental work should consider both geometrical and dynamical similarities in the experimental design.

Linear analysis defines the onset of instability. The next natural step is to describe the nonlinear evolution of the most unstable linear mode and attempt to reconcile the theoretical prediction with the observed shallow wake structures. Starting from the rigid-lid shallow-water equations and using the method of multiple scales, an amplitude evolution equation for the most unstable mode is derived. The resulting equation has complex coefficients and is of Ginzburg–Landau type. The complex coefficients of the equation are calculated and confirm the existence of a finite equilibrium amplitude, where the unstable mode evolves with time into a limit-cycle oscillation. This is consistent with the flow patterns observed by Ingram & Chu (1987), Chen & Jirka (1995), Balachandar *et al.* (1999), and Balachandar & Tachie (2001). In particular, Balachandar *et al.* (1999) classify the flows as deep–shallow wakes and shallow–shallow wakes on the basis of the presence or absence of the vortex street. Experiments show that deep–shallow wake flow patterns closely resemble the structure of deep two-dimensional bluff body wakes. The vortices in such cases are distinct and well organized; they increased in size downstream from the plate. The vortex street pattern is shown to be maintained over a large distance downstream (about 20 diameters for the experiments with a small cylinder in Chen & Jirka (1995) and about 200 plate widths for the experiments with a plate in Balachandar & Tachie (2001). Shallow–shallow wakes are characterized by relatively narrow wake regions. In addition, vortex street patterns either were not observed at all or appeared to be relatively weak and less organized in comparison with flows at larger depths. It is also found that the degree of variation from the classical vortex street flow increased downstream from the plate. Similar flow patterns were observed by Chen & Jirka (1995) (they classify the flows as vortex street, unsteady bubble and steady bubble). Reasonable agreement between the numerical data of Grubišić *et al.* (1995) and the linear and weakly nonlinear stability analysis provides further support that the finite-amplitude equilibrium structures in shallow wake flows which represent the transition from stable to convectively unstable wake may be described by the nonlinear Ginzburg–Landau equation. However, a definitive conclusion on the applicability of the Ginzburg–Landau type models for shallow wake flows is not possible at present for it requires detailed data on the spatial and temporal growth of the instability. Such data are currently not available.

REFERENCES

BALACHANDAR, R. & TACHIE, M. F. 2001 A study of boundary layer-wake interaction in shallow open channel flows. *Exps. Fluids* **30**, 511–521.

BALACHANDAR, R., RAMACHANDRAN, S. & TACHIE, M. F. 2000 Characteristics of shallow turbulent near wakes at low Reynolds numbers. *Trans ASME: J. Fluids Engng* **122**, 302–308.

BALACHANDAR, R., TACHIE, M. F. & CHU, V. H. 1999 Concentration profiles in shallow turbulent wakes. *Trans ASME: J. Fluids Engng* **121**, 34–43.

CHAUDHRY, M. H. 1993 *Open-channel Flows*. Prentice Hall.

CHEN, D. & JIRKA, G. H. 1995 Experimental study of plane turbulent wake in a shallow water layer. *Fluid Dyn. Res.* **16**, 11–41.

CHEN, D. & JIRKA, G. H. 1997 Absolute and convective instabilities of plane turbulent wakes in a shallow water layer. *J. Fluid Mech.* **338**, 157–172.

CHU, V. H., WU, J. H. & KHAYAT, R. E. 1991 Stability of transverse shear flows in shallow open channels. *J. Hydraul. Engng, ASCE* **117**, 1370–1388.

FALQUÉS, A. & IRANZO, V. 1994 Numerical simulation of vorticity waves in the nearshore. *J. Geophys. Res.* **99** (C1), 825–841.

FEDDERSEN, F. 1998 Weakly nonlinear shear waves. *J. Fluid Mech.* **372**, 71–91.

GHIDAOUI, M. S. & KOLYSHKIN, A. A. 1999 Linear stability analysis of lateral motions in compound open channels. *J. Hydraul. Engng, ASCE* **125**, 871–880.

GRUBIŠIĆ, V., SMITH, R. B. & SCHÄR, C. 1995 The effect of bottom friction on shallow-water flow past an isolated obstacle. *J. Atmos. Sci.* **52**, 1985–2005.

HANNEMANN, K. & OERTEL, H., JR 1989 Numerical simulation of the absolutely and convectively unstable wake. *J. Fluid Mech.* **199**, 55–88.

HUERRE, P. & MONKEWITZ, P. A. 1990 Local and global instabilities in spatially developing flows. *Annu. Rev. Fluid Mech.* **22**, 473–537.

HUERRE, P. & ROSSI, M. 1998 Hydrodynamic instabilities in open flows. In *Hydrodynamics and Nonlinear Instabilities* (ed. C. Godréche & P. Manneville). Cambridge University Press.

INGRAM, R. G. & CHU, V. H. 1987 Flow around islands in Rupert Bay: An investigation of the bottom friction effect. *J. Geophys. Res.* **92**, 14521–14533.

KEVORKIAN, J. & COLE, J. D. 1996 *Multiple Scale and Singular Perturbation Methods*. Springer.

KOLYSHKIN, A. A. & GHIDAOUI, M. S. 2002 Gravitational and shear instabilities in compound and composite channels. *J. Hydraul. Engng, ASCE* **128**, 1076–1086.

LEWEKE, T. & PROVANSAL, M. 1995 The flow behind rings: bluff body wakes without end effects. *J. Fluid Mech.* **288**, 265–310.

LIGGETT, J. A. 1994 *Fluid Mechanics*. McGraw-Hill.

LLOYD, P. M. & STANSBY, P. K. 1997 Shallow-water flow around model conical islands of small side slope. *J. Hydraul. Engng, ASCE* **123**, 1057–1067.

MATHIS, C., PROVANSAL, M. & BOYER, L. 1984 The Bénard–von Kármán instability: an experimental study near the threshold. *J. Phys Lett. Paris* **45**, L483–L491.

MONKEWITZ, P. A. 1988 The absolute and convective nature of instability in two-dimensional wakes at low Reynolds numbers. *Phys. Fluids* **31**, 999–1006.

NOACK, B. R. & ECKELMANN, H. 1994 A global stability analysis of the steady and periodic cylinder wake. *J. Fluid Mech.* **270**, 297–330.

PIER, B. 2002 On the frequency selection of finite-amplitude vortex shedding in the cylinder wake. *J. Fluid Mech.* **458**, 407–417.

PROVANSAL, M., MATHIS, C. & BOYER, L. 1987 Bénard-von Kármán instability: transient and forced regimes. *J. Fluid Mech.* **182**, 1–22.

SCHÄR, C. & SMITH, R. B. 1993a Shallow-water flow past isolated topography. Part I: Vorticity production and wake formation. *J. Atmos. Sci.* **50**, 1373–1400.

SCHÄR, C. & SMITH, R. B. 1993b Shallow-water flow past isolated topography. Part II: Transition to vortex shedding. *J. Atmos. Sci.* **50**, 1401–1412.

SCHLICHTING, H. 1979 *Boundary–layer Theory*, 7th Edn. McGraw-Hill.

SCHUMM, M., BERGER, E. & MONKEWITZ, P. A. 1994 Self-excited oscillations in the wake of two-dimensional bluff bodies. *J. Fluid Mech.* **271**, 17–53.

SOCOLOFSKY, S. A., VON CARMER, C. & JIRKA, G. H. 2003 Shallow turbulent wakes: Linear stability analysis compared to experimental data. In *Proc. Intl Symp. on Shallow Flows, Delft University of Technology, June 16–18, 2003*, Part I, pp. 133–140.

STEWARTSON, K. & STUART, J. T. 1971 A non-linear instability theory for a wave system in plane Poiseuille flow. *J. Fluid. Mech.* **48**, 529–545.

TACHIE, M. F. & BALACHANDAR, R. 2001 Shallow wakes generated on smooth and rough surfaces. *Exps. Fluids* **30**, 467–474.

TRIANTAFYLLOU, G. S., TRIANTAFYLLOU, M. S. & CHRYSSOSTOMIDIS, C. 1986 On the formation of vortex streets behind stationary cylinders. *J. Fluid. Mech.* **170**, 461–477.

VAN DYKE, M. 1982 *An Album of Fluid Motion*. The Parabolic Press.

WOLANSKI, E. J., IMBERGER, J. & HERON, M. L. 1984 Island wakes in shallow coastal waters. *J. Geophys. Res.* **89**, 10553–10569.

YAKUBENKO, P. A. & SHUGAI, G. A. 1999 Note on two-dimensional instability in shallow-water flows. *Acta Mechanica* **135**, 101–112.

ZWILLINGER, D. 1998 *Handbook of Differential Equations*, 3rd Edn. Academic.